1.

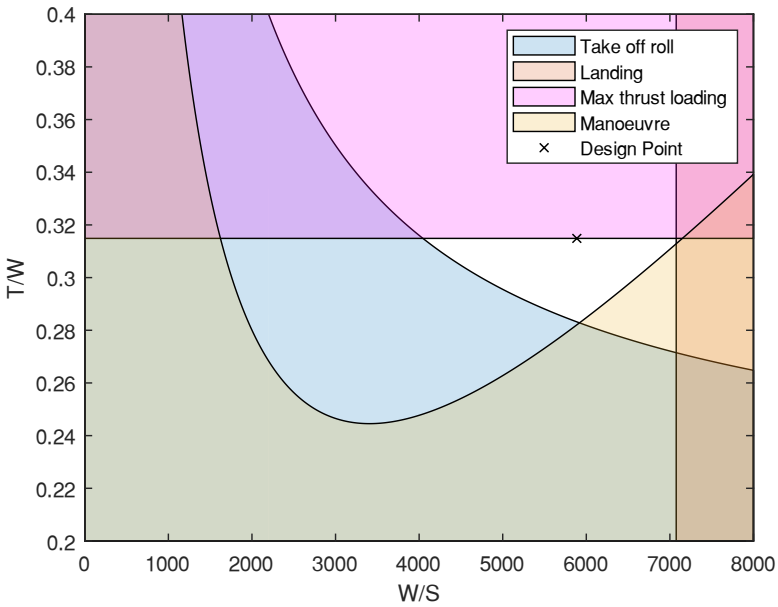

Figure 2.1.1: Constraint diagram of the aircraft

2. a.

Table 2.2.1: Parameters used in the analysis of the aircraft.

Speed (ms^{-1})	**Root Reynolds Number**	**Tip Reynolds Number**	**Density (kgm^{-3})**	**Temperature (°C)**	**Viscosity (m^2s^{-1})**	
230.412	71,595,106	21,452,685	0.562	-56.0	Kinematic	Dynamic
					1.783e-05	1.00e-05

The speed was calculated using the speed of sound at the cruise altitude of 35,000 feet which is 295.4 ms^{-1} [5] which is then multiplied by the cruise Mach number 0.79 which gives the speed 230.412 ms^{-1}. The root and tip Reynolds numbers, density and viscosity were calculated in XFLR5. The temperature at 35,000 feet was obtained from an online source [5].

b.

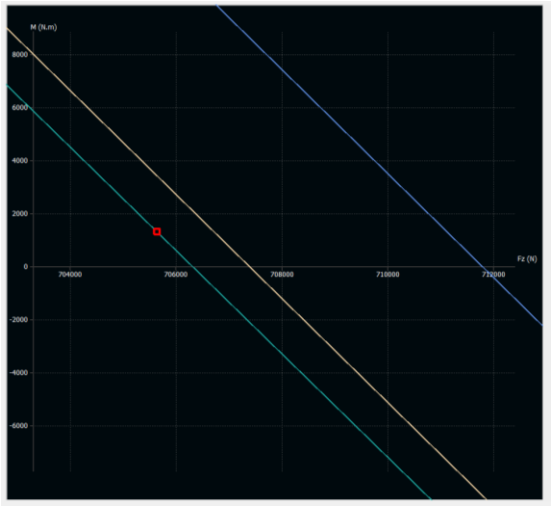

Figure 2.2.1: Moment (Nm) vs. F_Z (N) graph of trimmed aircraft (green) with elevator angle -0.2047 at angle of attack (red dot) compared to elevator -2.05 (blue) and elevator -2.05 (beige)

The stability modes were obtained for the trimmed aircraft in cruise. The values obtained are reported in Table 2.4.2. Overall, the aircraft modes are dynamically stable because as seen in Table 2.4.2 the damping ratios are all positive which is an indication of dynamic stability. This is also justified by the poles being in the top left corner of the s-plane with the point on the negative plane is just a reflection of that of the positive imaginary value.

The handling characteristics of the aircraft modes are discussed to assess the stability of the trimmed baseline aircraft. These are concerned with the short term and long-term handling characteristics. The short-term characteristics are defined as the short period dynamics modes and their influence on manoeuvrability. The long-term handling characteristics are defined as the ability to maintain the trimmed equilibrium state which is influenced by the long period dynamic modes [14]. The longitudinal short-term characteristics include the short period mode and the phugoid mode. The acceptable limits for the damping ratio of the short period mode are to be between 0.3 and 2 [14]. Therefore, the damping ratio of the short period mode is acceptable. It also states that the phugoid dynamics are acceptable if the mode is stable and the damping ratio is greater than 0.04. The lateral directional dynamic stability is comprised of the roll subsidence mode, spiral mode, and Dutch roll mode. The roll subsidence mode is crucial in determining the handling characteristics. The time constant of this aircraft's roll subsidence mode is 0.2s which is less than the maximum time constant of 1.4s [14] therefore it is handleable. The spiral mode's degree of instability is related to its time to double bank angle which for this aircraft is 309s which is much larger than the minimum value stated by Cook for an aircraft in cruise which is 20s therefore it is stable in terms of roll control force. The Dutch roll mode has a large influence on the lateral stability of the aircraft as it is a short period mode in the lateral direction. If the yaw damping is low, it is seen as a difficulty in handling rather than a serious problem [14]. The damping ratio of this mode is 0.147 and the minimum value acceptable by Cook is for aircraft in cruise is 0.08. The natural frequency is 3.9 rad/s and the minimum value is 0.5rad/s therefore the handling quality is acceptable.

To further discuss the stability and dynamics of the aircraft, it was compared to an already known aircraft with similar design characteristics. The aircraft chosen for comparison was the Airbus A320 because it has a main wingspan of 35 meters and an elevator span of 12.45 meters as well as a fin height of 5.87 meters [15].

Table 2.4.4: Comparison of longitudinal modes between A320 and aircraft

	A320		Baseline Aircraft	
	Natural frequency (Hz)	**Damping ratio**	**Natural frequency (Hz)**	**Damping ratio**
Short period	0.999	0.498	0.743471	0.347696
Phugoid	0.0937	0.171	0.00920179	0.0213786
Dutch Roll	1.39	0.165	0.643293	0.147088

Using the values of natural frequency and damping ratios of the short period and phugoid modes of the two aircrafts shown in Table 2.4.4, the response was plotted shown in Figures 2.4.1 and 2.4.2 below.

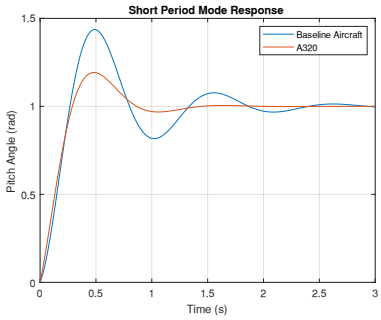

Figure 2.4.1: Response for short period mode

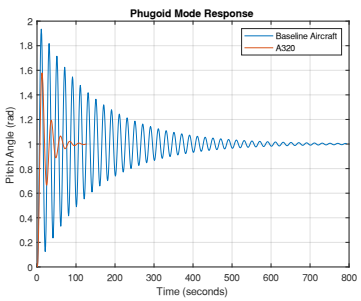

Figure 2.4.2: Response for phugoid mode

The short period and phugoid modes are both oscillatory aircraft modes. As seen in both Figures 2.4.1 and 2.4.2 the baseline aircraft has positive dynamic stability like the A320 as it settles to a certain value after a period of time. The baseline aircraft has a similar response for the short period mode as the A320 as they have similar natural

frequencies and damping ratios. They both take roughly similar times to settle, this means that the aircraft is as stable as the A320 in terms of achieving the trimmed condition after a disturbance to the pitch angle. As seen in Figure 2.4.2 above, the baseline aircraft has a settling time of almost 8 times greater than the A320 and has a much smaller damping ratio. Overall, it can be concluded that the baseline aircraft is less dynamically stable than the A320 in both the short period and phugoid longitudinal modes. For lateral modes, Figure 2.4.3 below shows the Dutch roll mode response for the A320 and the Baseline Aircraft. The A320 has a natural frequency approximately 2 times greater than the Baseline Aircraft however a similar damping ratio which is only 2% higher than the Baseline Aircraft. For both the roll and yaw angle, the A320 achieves the trimmed condition almost 5 times faster than the Baseline Aircraft as the A320 takes approximately 5-6 seconds while the Baseline Aircraft takes about 50 seconds. Both aircrafts take about 4 to 5 cycles to retrieve the stability condition.

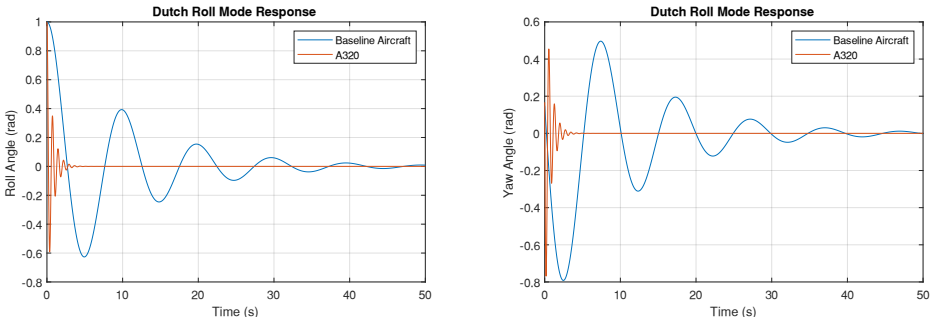

Figure 2.4.3: Dutch Roll response for roll angle and yaw angle (left to right)

5. Induced drag is calculated using the following formula:

$$D_i = \frac{1}{2}\rho V^2 S C_{D_i} \tag{6}$$

To reduce induced drag in cruise, there are several approaches in the design phase of an aircraft that could be taken. The Aspect Ratio (AR) of the wing could be increased to reduce the amount of induced drag experienced by the aircraft in cruise. This is because by increasing the AR of the wing, the wingspan typically increases which means that there is a greater distance for the air to travel to the wing tips where it sheds the vortices. These wing vortices tend to travel outwards to the wingtip and join so once the wingtip is reached there is a large wing tip vortex formed and it will shed. These vortices will increase the induced drag as explained in Q3. By increasing the wingspan there is further distance for the wing vortices to travel before shedding at the wing tip which causes the strength and size of the vortex to reduce hence the induced drag is reduced.

Another change that could be made is to alter the Taper Ratio (TR) of the wing. By increasing the taper of the wing, it means to increase the ratio of the chord at the wing root to the chord at the wing tip. If the wing has more taper, there will be less distribution of lift at the wing tip leading to smaller wing tip vortices causing less induced drag. A problem that could rise from over tapering the wing is that wing tip stall is likely to occur in highly tapered wings due to the lift distribution being at a maximum near the tip.

Additionally, the twist of the wing could be altered to reduce induced drag. By giving the wing twist, the angle of attack across the span of the wing varies. A wing is said to have ‘washout’ when the angle of incidence as the wing tip is lower than that at the wing root. This is useful because a lower angle of incidence will correspond to a lower amount of lift produced hence the drag acting against that lift is reduced. The main purpose of washout in a wing is to control the stall characteristics. By having washout, it causes the root to stall before the tip which allows the aircraft to maintain in flight without experiencing bad stall effects.

Finally, winglets could be added to reduce induced drag as they produce a forward thrust inside the circulation field of the vortices which reduce their strength [16]. With weaker vortices, induced drag is reduced and the overall efficiency of the aircraft is increased.

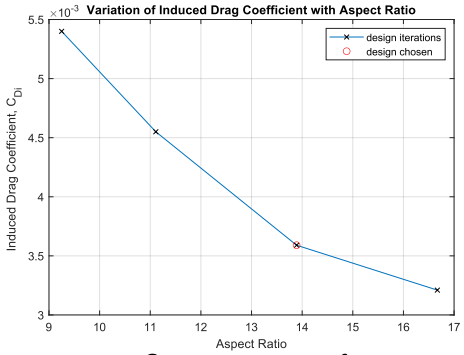

Figure 2.5.1: C_{D_i} per iteration of Aspect Ratio

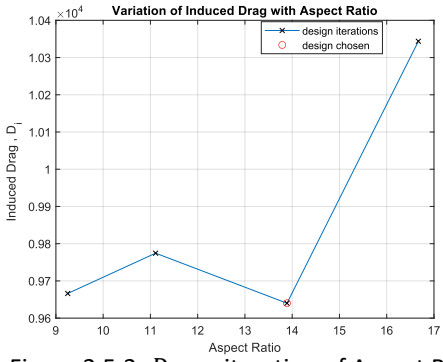

Figure 2.5.2: D_i per iteration of Aspect Ratio

After obtaining the optimal aspect ratio, the winglets on the aircraft were added to this design. The dimensions of them are described in the dimensioned diagram in figure 2.5.5. the induced drag coefficients were tested for different angles of the winglets offset from the vertical: 0°, 30° and 60°. The addition of winglets does cause the aspect ratio and wing area to increase however it is assumed that this does not increase the MTOW by a significant amount. Therefore, the values for each iteration of winglet angle are reported in Table 2.5.2.

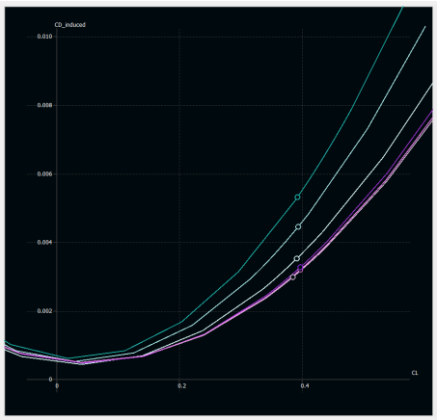

Figure 2.5.3: C_{D_i} against C_l graph from XFLR5 showing the effect of changing the aspect ratio (green shades) and adding winglets (purple shades)

Table 2.5.2: Summary of values used to obtain the induced drag.

winglet angle °	S	$C_{l_{trim}}$	alpha	C_{D_i}	D_i	$C_{D_{viscous}}$
0	187.202	0.40362	2.64	0.00338	9439.384825	0.00690
30		0.40345	2.66	0.00331	9243.894607	0.00677
45		0.39039	2.52	0.00307	8573.64243	0.00670
60		0.39418	2.56	0.00311	8685.35	0.00667

After performing 4 iterations of winglet angles it was found that the angle of 45° produced a minimum induced drag coefficient and induced drag value. As the winglet angle increased past 45° it is noticed that the C_{D_i} starts to increase again. Therefore, the angle of 45° was chosen as the optimal design iteration because the induced drag coefficient and induced drag reduces by 9.2% overall. Graphs of the progression of induced drag coefficient and induced drag against winglet angle are plotted in figure 2.5.4 and 2.5.5 respectively.

After running a stability analysis for each of the planes with varying winglet angles, it is seen from table 2.5.3 that there are slight changes to the dynamic stability modes. Comparing the modes of the final design to that of question 4, it can be seen that the short period ω_n reduces by 13.4%, phugoid ω_n increases by 19.5% and Dutch roll reduces by 15.2%. The roll subsidence eigenvalue becomes more negative and spiral mode becomes slightly more positive. This means that the overall dynamics stability remains fairly the same, but the responses of the modes will differ for the oscillatory modes. For the non-oscillatory modes, the stability improves as they are placed better in the top left corner of the s-plane based on their eigenvalues.

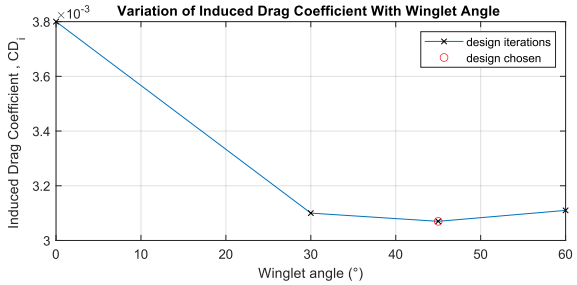

Figure 2.5.4: C_{D_i} vs winglet angle

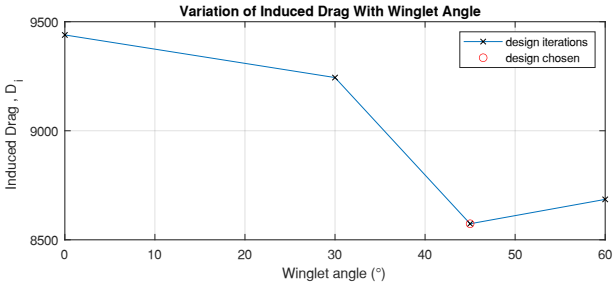

Figure 2.5.4: D_i vs winglet angle

Table 2.5.3: Summarising the dynamic aircraft modes for each AR. $\omega_n = natural\ frequency, \zeta = damping\ ratio$

Winglet angle (°)	Short period		Phugoid		Dutch roll		Roll subsidence	Spiral
	ω_n (Hz)	ζ	ω_n (Hz)	ζ	ω_n (Hz)	ζ	Eigenvalue	Eigenvalue
0	0.614537	0.389	0.011045	0.016	0.483877	0.132	-6.646 + 0.00i	-0.0004 + 0.00i
30	0.626673	0.381	0.011895	0.016	0.541975	0.155	-7.106 + 0.00i	-0.0008 + 0.00i
45	0.643537	0.378	0.011066	0.016	0.545788	0.157	-7.474 + 0.00i	-0.0006 + 0.00i

Table 2.5.4: Summarising the points of stability for each AR. MAC =3.852

Winglet angle	Neutral point (m)	CoG X (m)	Static margin (m)	% of MAC
0	18.188	16.98	1.208	31.36
30	18.243		1.263	32.78
45	18.269		1.289	33.46

The static stability of the aircraft with the variation of winglet angle is shown in Table 2.5.4. As the winglet angle increases, the neutral point increases resulting in the static margin increases. Comparing the static margin as a percentage of MAC with that of the original aircraft from question 4, the value reduces from 48.7% to 33.46% which is a 31.3% reduction showing that the elevator authority is improved with this final design.

The Oswald Efficiency Factor e was recalculated for the new optimised design which is 0.977 while the original design is 0.95. Since the new value is closer to $e = 1$ which is for an ellipse, the new value is better as an elliptic lift distribution produces less drag.

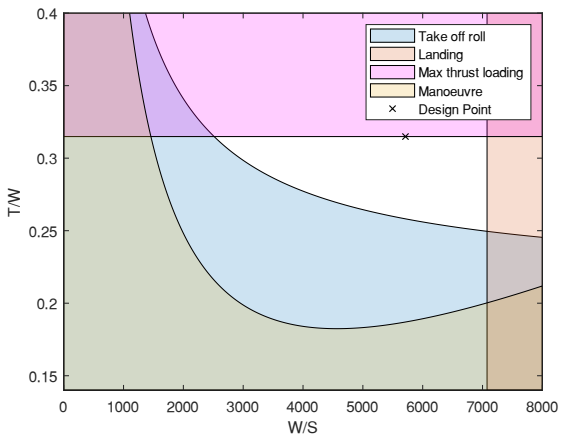

Figure 2.5.4: updated constraint diagram

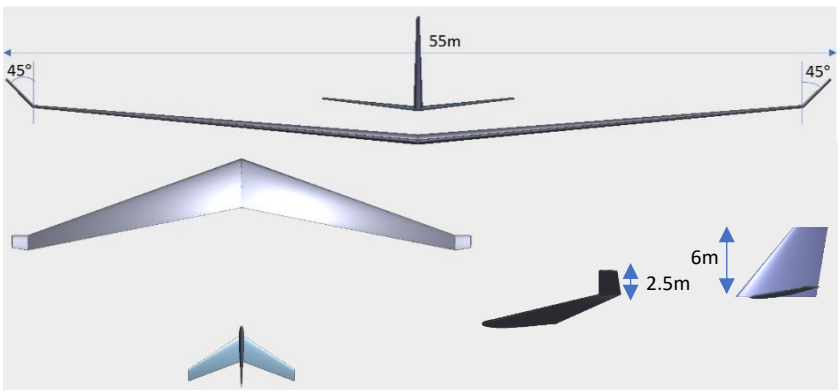

Figure 2.5.5: dimensioned diagram showing changes made.